RSC Advances

PAPER

View Article Online
View Journal | View Issue

Cite this: *RSC Adv.*, 2020, **10**, 18054

An ultra-sensitive T_2-weighted MR contrast agent based on Gd^{3+} ion chelated Fe_3O_4 nanoparticles

Jing Chen,[a] Hui-Hui Xiang,[ab] Zu-Zhi Zhao,[a] Yun-Kai Wu,[a] Meng-Yu Fei[c] and Meng-Meng Song *[a]

Received 25th February 2020
Accepted 24th April 2020

DOI: 10.1039/d0ra01807d

rsc.li/rsc-advances

An ultra-sensitive T_2-weighted MR imaging contrast agent was prepared based on Fe_3O_4 nanoparticles and Gd^{3+} ions (Fe_3O_4@Gd). Amino modified Fe_3O_4 nanoparticles were conjugated to diethylenetriamine pentaacetic acid, and finally coordinated with Gd^{3+} ions. The nanoparticles had a uniform morphology with a size of 100 nm and a Gd/Fe mass ratio of 1/110. The r_2 (transverse relaxivity) of the Fe_3O_4 nanoparticles increased from 131.89 mM^{-1} s^{-1} to 202.06 mM^{-1} s^{-1} after coordination with Gd^{3+} ions. MR measurements showed that the aqueous dispersion of Fe_3O_4@Gd nanoparticles had an obvious concentration-dependent negative contrast enhancement. Hepatoma cells were selected to test the cytotoxicity and MR imaging effect. The application of Fe_3O_4@Gd nanoparticles as contrast agents was also exploited *in vivo* for T_2-weighted MR imaging of rat livers. All the results showed the effectiveness of the nanoparticles in MR diagnosis.

Introduction

Early and highly accurate diagnosis has great significance in modern medicine.[1] Magnetic resonance imaging (MRI) has been the most powerful and effective diagnostic method due to its many advantages, such as few side effects and non-invasive properties.[2–4] MR contrast agents have played an important role in improving sensitivity by enhancing the contrast between normal tissue and diseased tissue.[5] The commonly used MR contrast agents are divided into T_1-positive agents, such as Gd chelates, and T_2-negative agents, such as superparamagnetic iron oxide Fe_3O_4 nanoparticles.[6]

High transversal relaxation is necessary for MR contrast agents. For the past few years, a lot of effort has been devoted to the development of novel ultra-sensitive contrast agents.[5,7,8] Some researchers tried to use materials of high saturation magnetization (M_s) as an alternative, such as $MnFe_2O_4$ and $CoFe_2O_4$.[9,10] Because the size, shape and surface modification affected the saturation magnetization of nanoparticles, nanoparticles with cube, octapod, rod and other non-spherical shapes had been also exploited as ultrasensitive contrast agents.[11,12] In addition to the intrinsic materials properties, r_2 enhancement can also be realized by developing aggregates or clusters of magnetic nanoparticles.[13–15] Recently, Huang *et al.* enhanced the transversal relaxation of Fe_3O_4 nanoparticles by using Gd^{3+}-chelated mesoporous silica shells.[16] Enlightened by this, we designed a facile strategy to prepare nanoparticles based on Fe_3O_4 nanoparticles and Gd^{3+} ions. It is well known that Gd^{3+} ions have well coordination with diethylenetriaminepentaacetic acid (DTPA), so many scientists are working on how to conjugate DTPA to Fe_3O_4 nanoparticles. To achieve this goal, chemicals contain amino group have been used to modify Fe_3O_4 nanoparticles and then coupled to DTPA *via* chemical conjugation or electrostatic interaction, such as (3-aminopropyl)triethoxysilane (APS), dopamine, chitosan and polyethyleneimine (PEI).[16–18] Here amino group modified Fe_3O_4 nanoparticles were hydrothermal synthesized and then the nanoparticles were further modified by DTPA, which enabled the following chelation with Gd^{3+} ions. Besides, the relaxivity increased from 131.89 mM^{-1} s^{-1} of Fe_3O_4 to 202.06 mM^{-1} s^{-1} of Fe_3O_4@Gd nanoparticles while the previous publications reported Gd^{3+} chelated Fe_3O_4 nanoparticles always resulted in a decrease of relaxivity.[19]

The morphology, size and magnetic properties of the formed Fe_3O_4@Gd nanoparticles were characterized by TEM (transmission electron microscopy), DLS (dynamic light scattering) and VSM (vibrating sample magnetometer). The cytotoxicity and cellular uptake were also investigated by 3-[4,5-dimethylthiazol-2-yl]-2,5-diphenyl tetrazolium bromide (MTT) assay and Prussian blue staining method. The effectiveness of Fe_3O_4@Gd nanoparticles as MR contrast agents was investigated both *in vitro* and *in vivo*.

[a]*School of Basic Medical Sciences, Anhui Medical University, 81 Meishan Road, 230032 Hefei, Anhui, PR China. E-mail: songmengmeng@ahmu.edu.cn; Tel: +86-551-6516-1138*

[b]*Department of CT/MRI, Anhui No. 2 Provincial People's Hospital, 1868 Dangshan Road, North Second Ring Road, 230032 Hefei, Anhui, PR China*

[c]*The First Affiliated Hospital, Anhui Medical University, 218 Jixi Road, Hefei, Anhui, PR China*

Materials and methods

Chemicals and reagents

MTT, iron(III) chloride hexahydrate ($FeCl_3 \cdot 6H_2O$), DTPA, gadolinium(III) nitrate hexhydrate [$Gd(NO_3)_3 \cdot 6H_2O$], *N*-(3-dimethylaminopropyl)-*N*′-ethyl carbodiimide hydrochloride (EDC·HCl)

and *N*-hydroxysuccinimide (NHS) were purchased from Aladdin (Shanghai, China). HepG2 (liver hepatocellular carcinoma) cells were purchased from the Type Culture Collection of the Chinese Academy of Sciences (Shanghai, China). Sprague-Dawley rats (200–220 g) were purchased from Anhui Experimental Animal Center (Hefei, China).

Preparation of Fe_3O_4@Gd nanoparticles

Amino modified Fe_3O_4 nanoparticles are prepared according to Li *et al.*'s publication.[20] Briefly, 6.5 g 1,6-hexanediamine, 2.0 g anhydrous sodium acetate and 1.0 g $FeCl_3 \cdot 6H_2O$ were dissolved in 30 mL glycol and then transferred into a Teflon lined autoclave and kept at 190 °C for 6 h. The products were then washed with ethanol for many times. And then the nanoparticles are reacted with DTPA with the presence of EDC and NHS in MES buffer under room temperature for 72 h. After that, $Gd(NO_3)_3$ were added to the mixture and then stirred for another 24 h. Finally, the nanoparticles were collected by centrifugation and rinsed with water for many times.

Characterization of nanoparticles

The morphology of Fe_3O_4 nanoparticles and Fe_3O_4@Gd nanoparticles were characterized by TEM (JEOL, JEM-2100F). DLS measurement was determined by Zetasizer (Nano series, Malvern Instruments). The magnetic measurement was carried out using VSM (MPMS SQUIDM, USA). T_2-weighted MR imaging of Fe_3O_4 nanoparticles and Fe_3O_4@Gd nanoparticles were measured by an MR scanner at 3.0 T (GE, Milwaukee, USA) as follows: echo time (T_E) = 20, 40, 60, 80, 100 and 120 ms; repetition time (T_R) = 3000 ms; field of view (FOV) = 20 mm × 20 mm; slice thickness = 4.0 mm; matrix = 320 × 320. IR characterization was performed by an IR spectrometer (Nicolet iN10, Thermo scientific, USA).

In vitro study

Cell culture. HepG2 cells were cultured in RPMI 1640 medium with 10% fetal bovine serum (FBS), 100 mg mL^{-1} streptomycin, and 100 U mL^{-1} penicillin at 37 °C under 5% CO_2.

Cytotoxicity study. For MTT study, HepG2 cells were seeded on a 96-well plate at a density of 1×10^4 cells per well with. After 24 h, the culture medium was replaced with 100 μL of medium containing 0–40 μg mL^{-1} of Fe_3O_4@Gd nanoparticle. The cytotoxicity was evaluated by determining the cell viability after incubation for 24 h.

Prussian blue staining. HepG2 cells (5×10^5) were seeded in 6-well plates and then Fe_3O_4@Gd nanoparticles was added with the concentration range of 0–40 μg mL^{-1}. After 24 h, the cells were then treated with 4% formaldehyde for 30 min. Then 5% potassium ferrocyanide and 5% hydrochloric acid was added. Finally, cells were imaged by a microscope (Olympus, IX71).

MRI investigation. HepG2 cells (5×10^5) were plated in 6-well plates and then Fe_3O_4@Gd nanoparticles were added at a concentration of 0–40 μg mL^{-1}. After incubation for 24 h, the cells were collected and re-suspended in 0.5% agarose gel and then imaged by using a 3.0 T MR system (Discovery MR750w, GE Medical Systems, Milwaukee, WI, USA).

In vivo study

Animals. Sprague-Dawley rats (200–220 g) were purchased from the Anhui Experimental Animal Center with the license number "SCXK (Wan) 2011-002". The rats were housed under at 22 °C with a 12 h light/dark cycle and were allowed free access to food and water. All animal procedures were performed in accordance with the Guidelines for Care and Use of Laboratory Animals of Anhui Medical University and approved by the Animal Ethics Committee of Anhui Medical University.

Prussian blue staining. Liver, heart, spleen, kidney and lung tissues freshly removed from Fe_3O_4@Gd nanoparticles treated rat were fixed in 4% paraformaldehyde and processed routinely into paraffin, sectioned at a thickness of 3 μm, brain sections were then stained with Prussian blue and counterstained with eosin. Finally, the sections were imaged by a microscope (Olympus, IX71).

MRI investigation. For *in vivo* MR investigation, SD rats were tail vein injected with Fe_3O_4@Gd nanoparticles (1 mL, 10 mg per kg of rat body weigh). The rats were imaged before and at 0.5 h, 1 h, and 24 h post injection. T_2-weighted MR images were

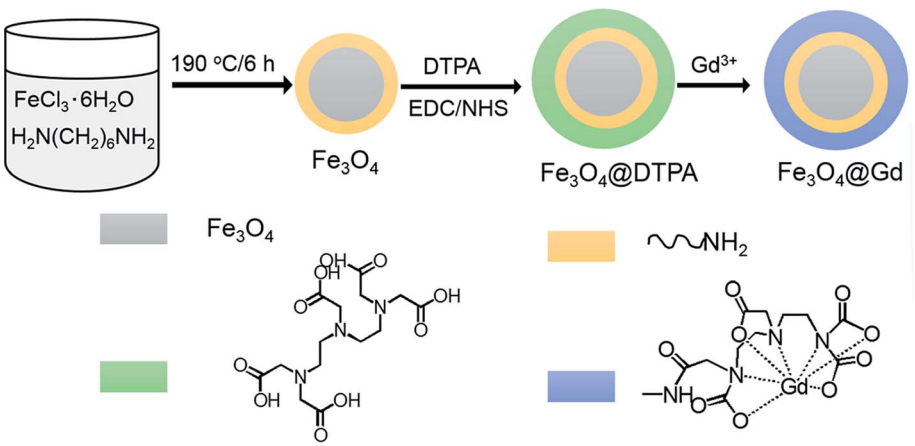

Scheme 1 Schematic illustration of the formation of Fe_3O_4@Gd nanoparticles.

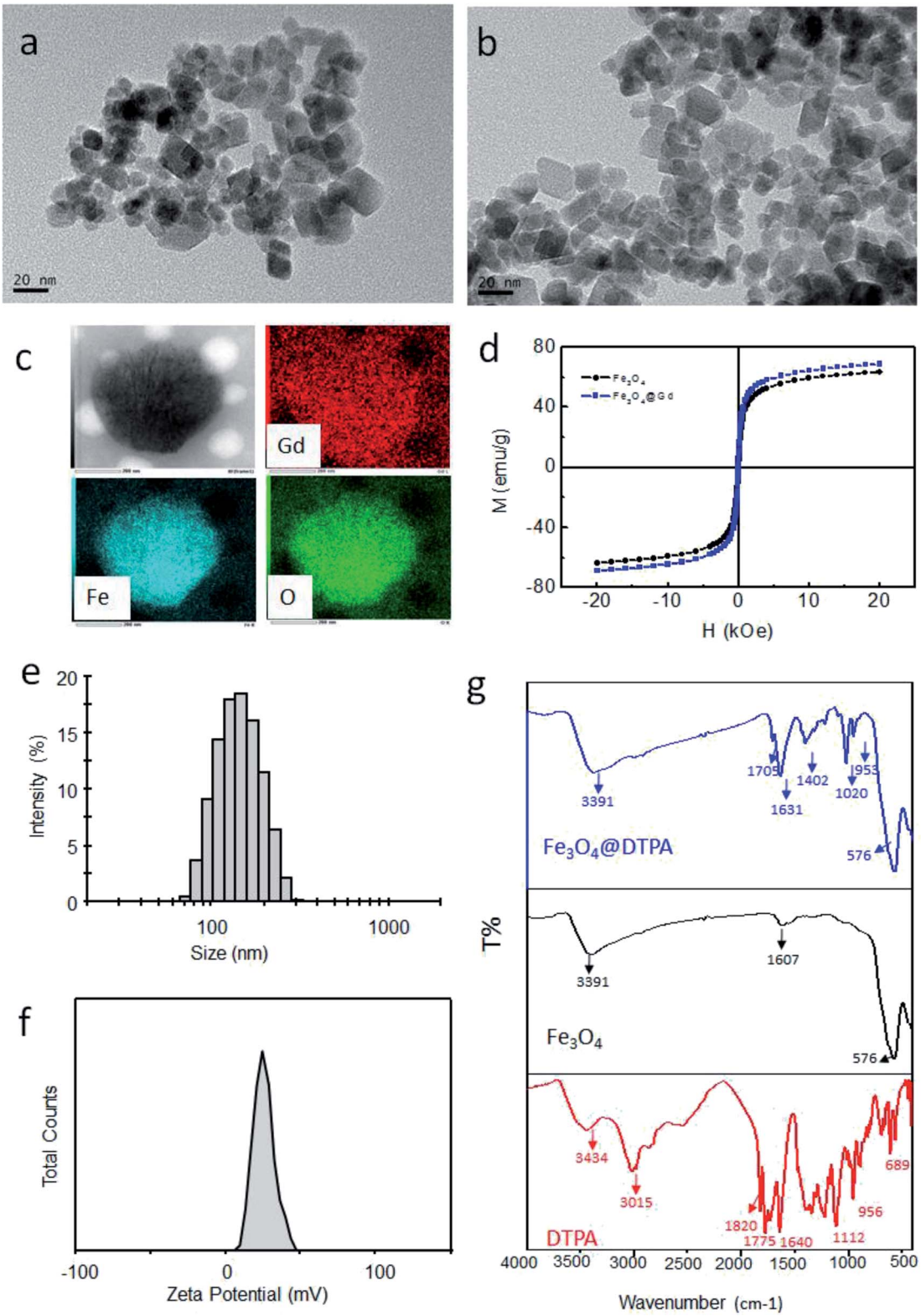

Fig. 1 Characterization of nanoparticles. (a) TEM image of Fe_3O_4 nanoparticles; (b) TEM image of Fe_3O_4@Gd nanoparticles; (c) EDX mapping images of one nanoparticle; (d) the magnetic hysteresis loops of Fe_3O_4 and Fe_3O_4@Gd nanoparticles at room temperature; (e) size distribution of Fe_3O_4@Gd nanoparticles; (f) zeta potential of Fe_3O_4@Gd nanoparticles; (g) IR spectra of Fe_3O_4@DTPA nanoparticles, Fe_3O_4 nanoparticles and DTPA.

obtained with a matrix size of 256 × 256, slice thickness of 2 mm, and field of view of 60 mm × 60 mm. The signal intensity was also measured.

Results

Materials characterization

Fe_3O_4@Gd nanoparticles were fabricated by three steps (Scheme 1). First, amino group modified Fe_3O_4 nanoparticles were hydrothermal synthesized. Second, DTPA were conjugated to amino group through amide bond. Finally, Gd^{3+} ions were chelated with DTPA to form Fe_3O_4@Gd nanoparticles. Fig. 1a and b showed the TEM images of Fe_3O_4 nanoparticles and Fe_3O_4@Gd nanoparticles, respectively. There was no obvious change between the morphology of the two samples, which had a size ranging from 10–50 nm. To confirm the element composition, energy-dispersive X-ray (EDX) element mapping was performed on a single nanoparticle (Fig. 1c). The results suggested that Gd element is present in the nanoparticle. Inductively coupled plasma atomic emission spectroscopy (ICP-AES) analysis was employed to quantify Fe and Gd content and the results showed the mass ratio of Gd/Fe is 1 : 110. According to the ICP analysis results, each nanoparticles have conjugated to 1.48×10^4 DTPA molecules.

The magnetic properties of the nanoparticles were measured at room temperature. As shown in Fig. 1d, the saturation magnetization value of Fe_3O_4 and Fe_3O_4@Gd nanoparticles are 63.35 emu g^{-1} and 68.65 emu g^{-1}, respectively. After chelated with Gd^{3+} ions, the saturation magnetization increased. Besides, both the values were lower than that of bulk Fe_3O_4, which was reasonable because the particle size decreased.[20] The remanence and coercivity of both the samples were nearly zero, suggesting the superparamagnetic property of the nanoparticles.

DLS measurements were carried out to measure the size and zeta potential values of the obtained nanoparticles. The hydrodynamic diameter histogram and the zeta potential distribution were presented in Fig. 1e and f. It was noticed that the hydrodynamic size of the nanoparticles was kept around 130 nm, which was larger than that obtained from TEM observation. This might be explained that the small nanoparticles aggregated slightly. However, the aggregates still had a proper size less than 200 nm, which was still proper for bio-applications. It was also worth mentioned that the obtained nanoparticles possessed a zeta potential of +17 mV, which was critical for formation of stable dispersions.

Fig. 1g shows the IR spectra of Fe_3O_4 nanoparticles before and after conjugated to DTPA and free DTPA. It can be see clearly that all the peaks of DTPA are appeared in the spectrum of the conjugated nanoparticles (Fe_3O_4@DTPA) with suppressed intensity. The adsorption peak at around 576 cm^{-1} was the characteristic absorption of Fe–O bond. Besides, there is a new peak at 1704 cm^{-1}, which is ascribed to C=O group of the formatted amide bond. All of these confirmed that DTPA is successfully conjugated to the surface of Fe_3O_4 nanoparticles *via* amide bond.

T_2 MR relaxometry

To investigate the possibility of Fe_3O_4@Gd nanoparticles as T_2-weighted contrast agents, MRI investigation were carried. Fig. 2

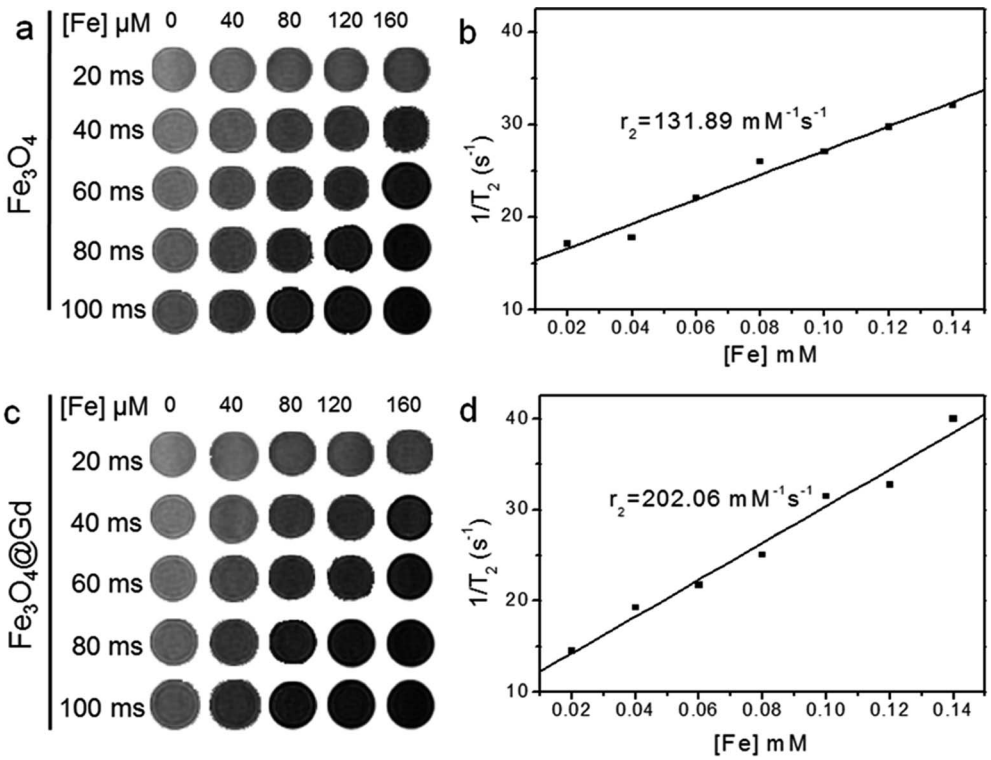

Fig. 2 T_2-weighted MR images at different Fe concentration in 0.5% agarose gel at different TE time and the analysis of relaxation rate *vs.* Fe concentration. (a and b) Fe_3O_4 nanoparticles. (c and d) Fe_3O_4@Gd nanoparticles.

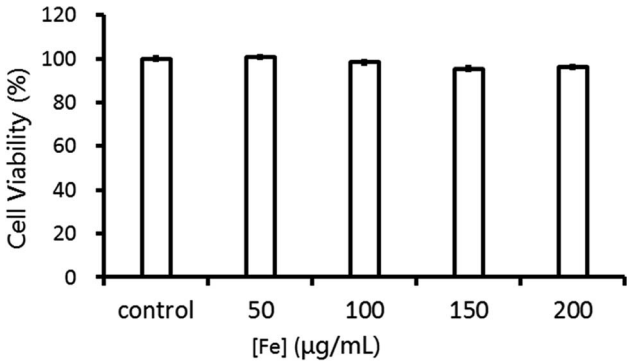

Fig. 3 Cell viability of HepG2 cells incubated with Fe_3O_4@Gd nanoparticles at various Fe concentrations.

showed the T_2-weighted MR images of Fe_3O_4 and Fe_3O_4@Gd nanoparticles with various Fe concentrations under different TE time. We observed that the T_2-weighted MR signal decreased with the increase of Fe concentration. Fe_3O_4@Gd nanoparticles exhibited much higher T_2-negative contrast than Fe_3O_4 nanoparticles. The scatter diagram of relaxation rate *vs.* concentration was linear fitted and the slope was equal to the transverse relaxivities r_2. The r_2 value of Fe_3O_4@Gd nanoparticles was measured to be 202.06 mM^{-1} s^{-1}, higher than that of Fe_3O_4 nanoparticles without Gd^{3+} ions coordination.

Cytotoxicity and cellular uptake studies

The biocompatibility is a critical parameter for materials in biomedical application. MTT assay was performed to evaluate the cell viability of HepG2 cells incubated with Fe_3O_4@Gd nanoparticles. As shown in Fig. 3, there was no obvious concentration-effect observed in [Fe] range of 50–200 μg mL^{-1}. After co-incubated with Fe_3O_4@Gd nanoparticles for 24 h, the cell viability with the highest concentration up to 200 μg mL^{-1} had no significant difference. This suggested that Fe_3O_4@Gd nanoparticles were very low toxic at the tested concentration range, which is beneficial for the further bio-medical applications.

To study the cellular uptake of Fe_3O_4@Gd nanoparticles, HepG2 cells incubated with Fe_3O_4@Gd nanoparticles with various concentrations were stained by Prussian blue and Eosin. Iron can be stained by Prussian blue and show blue color. As shown in Fig. 4a, HepG2 cells incubated with DMEM exhibited pink color. After incubated with Fe_3O_4@Gd nanoparticles, blue color were observed because of the internalized nanoparticles. The blue color also showed concentration-effect, as the concentration increased, the blue color became stronger. It was noteworthy that the blue color was located in the cytoplasm instead of nucleus, which suggested the internalized Fe_3O_4@Gd nanoparticles were mainly distributed in cytoplasm.

The MR imaging ability of Fe_3O_4@Gd nanoparticles was first performed *in vitro*. HepG2 cells were incubated with Fe_3O_4@Gd nanoparticles with various concentrations for 24 h and then collected for MR scanning. As shown in Fig. 5a, HepG2 cells after incubated with Fe_3O_4@Gd nanoparticles displayed a negative enhancement. The MR images of HepG2 cells darkened gradually as Fe concentration increased. HepG2 cells exposed to Fe_3O_4@Gd nanoparticles exhibited an obvious signal decrease even at the lowest concentration 5 μg mL^{-1}

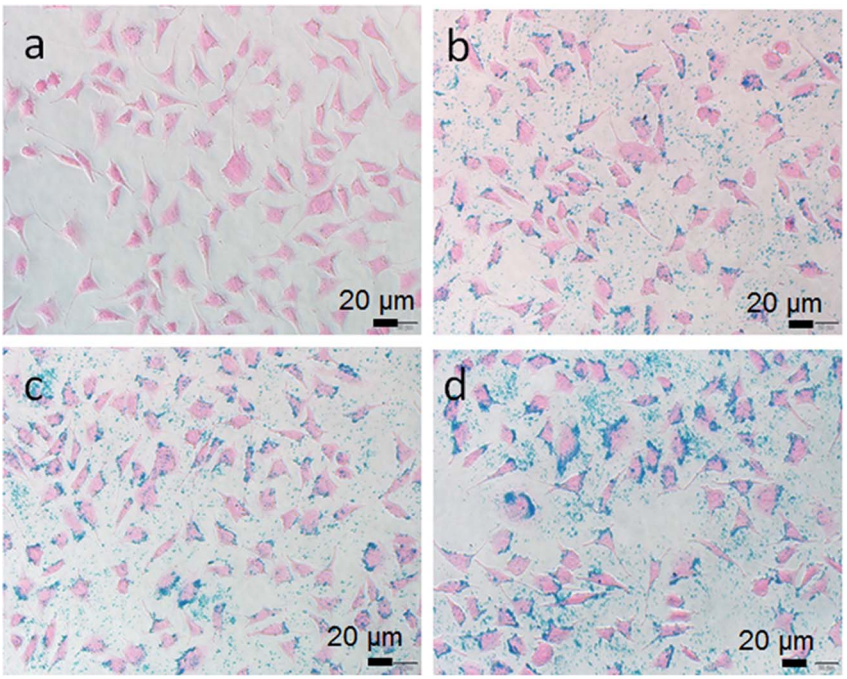

Fig. 4 Prussian blue staining images of HepG2 cells incubated with Fe_3O_4@Gd nanoparticles at various iron concentration ((a) – control, (b) – 10 μg mL^{-1}, (c) – 20 μg mL^{-1}, (d) – 30 μg mL^{-1}).

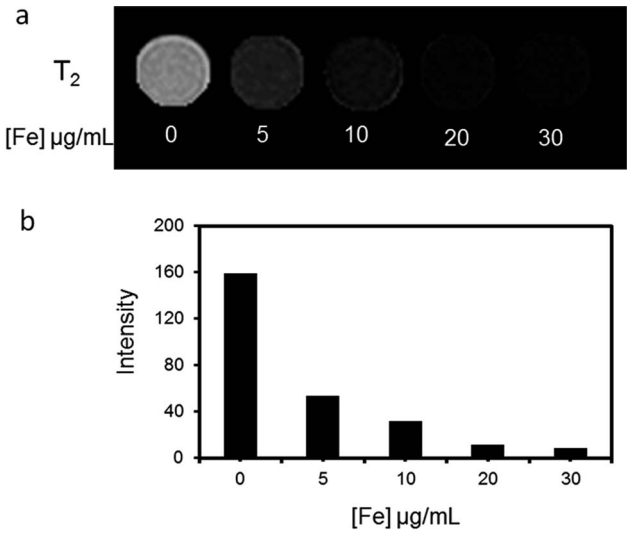

Fig. 5 MR investigation *in vitro*. (a) T_2-weighted MR images of HepG2 cells incubated with Fe_3O_4@Gd nanoparticles with iron concentration ranging from 0–30 μg mL^{-1} and (b) the corresponding analysis of MR signal intensity.

compared with control cells. When iron concentration greater than 20 μg mL^{-1}, the signal intensity was almost keep stable. This demonstrated that the uptake of Fe_3O_4@Gd nanoparticles of HepG2 cells was nearly saturated.

MR investigation

High r_2 relaxivity, low toxicity and good imaging effect *in vitro* encouraged us to explore there *in vivo* T_2-weighted MR imaging capability. 10 mg Fe_3O_4@Gd nanoparticles (1 mL, 10 mg per kg of rat body weight) were injected into the SD rat *via* tail vein. After vein tail injection of our nanoparticles, MR scanning was performed. Fig. 6 showed T_2-weighted MRI images of rat liver collected from different time. After injection 30 min, MR images of liver showed slightly changes. The signal intensity of the corresponding T_2-weighted images was plotted in Fig. 6e. As long prolonged, the T_2 MR signal intensity of liver darkened gradually compared with that before injection. At 24 h post injection, the rat liver showed the lowest signal intensity in T_2-weighted MR images. This result demonstrated that the negative enhancement of MRI could be achieved by using our Fe_3O_4@Gd nanoparticles as contrast agents.

In vivo biodistribution

Prussian blue staining was used to investigate the *in vivo* biodistribution of the Fe_3O_4@Gd nanoparticles. At 24 h post-injection, different organs including heart, liver, spleen, lung, and kidney were harvested and then stained by Prussian blue and Eosin (Fig. 7). As shown Fig. 7a and magnified Fig. 7b, it is obvious that large amounts of nanoparticles distributed in the liver, which suggested large amount of Fe_3O_4@Gd uptake in the liver. A relatively small amount of Fe_3O_4@Gd uptake can also be found in the other organs, such as lung and kidney. There is almost no Fe_3O_4@Gd uptake in heart and lung.

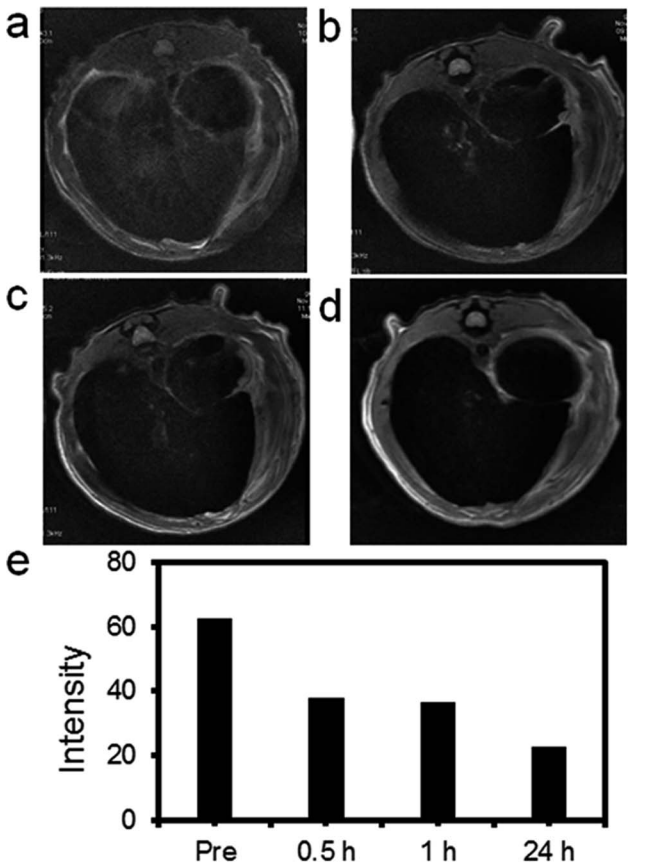

Fig. 6 MR images of rat liver before and after vein tail injection of Fe_3O_4@Gd nanoparticles (10 mg kg^{-1}). (a) Pre-injection; (b) 30 min after injection; (c) 60 min after-injection; (d) 24 h after injection; (e) the corresponding T_2-weighted MR signal intensity of the liver.

Discussion

Here we prepared Gd^{3+} ions chelated Fe_3O_4 nanoparticles as contrast agent for T_2-weighted MR imaging. Between the two components, one is T_1 positive contrast agent and the other is T_2 negative contrast agent. For the previous publications, the integration of these two components for MR contrast agents is mainly utilized as T_1- and T_2-dual mode MR contrast agent.[21–23] For instance, Bae, *et al.* reported a dual mode contrast agent Gd(DTPA) labelled IONP has r_2 value of 30.32 mM^{-1} s^{-1} and r_1 value of 11.17 mM^{-1} s^{-1} at 3.0 T with similar size.[19] Thorat *et al.* reported a multifunctional gadolinium-doped iron oxide nanoparticles for targeted magnetic hyperthermia, chemotherapy and T_1–T_2 dual-model magnetic resonance (MR) imaging with r_2 value of 50.47 mM^{-1} s^{-1} and r_1 value of 1.55 mM^{-1} s^{-1} at 3.0 T.[24]

A similar formulation based on Fe_3O_4 and Gd^{3+} has also been reported, Gd^{3+} ions were introduced *via* three different methods including direct complex formation, covalent attachment and electrostatically and the results indicated only the nanoparticles

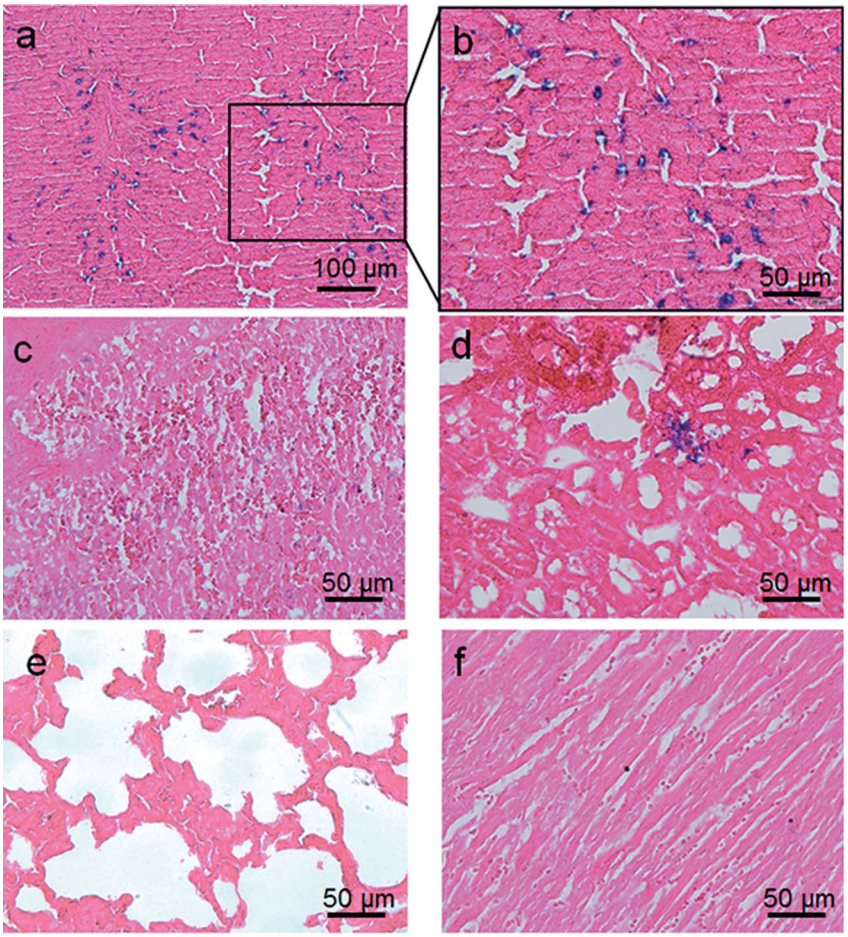

Fig. 7 Prussian blue staining images of the major organs of SD rats ((a and b) – liver, (c) – spleen, (d) – kidney, (e) – lung and (f) – heart). The sections were acquired from rat at 24 h after intravenous injection of 10 mg kg^{-1} Fe_3O_4@Gd nanoparticles.

obtained by the following two methods work effective.[25] Here Fe_3O_4@Gd nanoparticles were prepared by a very facile conjugate method. Amino modified Fe_3O_4 nanoparticles were prepared by one-pot hydrothermal synthesis method and then coupled to DTPA and further chelated with Gd^{3+} ions. The r_2 of Fe_3O_4@Gd nanoparticles (202.06 mM^{-1} s^{-1}) is higher than that of Fe_3O_4 nanoparticles (131.89 mM^{-1} s^{-1}). However, the introduction of Gd^{3+} has no obvious contribution for the enhancement of longitudinal relaxivity r_1, which is only 1 mM^{-1} s^{-1}. This may be explained by the low content of Gd in our nanoparticles. This different influence of Gd^{3+} to longitudinal relaxivity and transverse relaxivity are also found by Huang *et al.*[16] Recently, some scientists proposed to classify a contrast agent with $r_2/r_1 > 10$ as T_2 agents.[26] Therefore, we named the Fe_3O_4@Gd nanoparticles as T_2 contrast agents. The reason why transverse relaxivity increased are not clear.

There are many factors affect the relaxivities, such as particle size, aggregation and surface modification. Therefore it is difficult to compare our nanoparticle to other formulation. However, the r_2 relaxivity of Fe_3O_4@Gd nanoparticles is higher than that of commercialized Feridex r_2 (148.95 mM^{-1} s^{-1}),[19] suggesting their T_2 contrast effect was strong enough to be qualified as T_2-weighted MR contrast agents.

It is important to understand the biodistribution of the fabricated Fe_3O_4@Gd nanoparticles for their bio-medical applications. The particles are mainly distributed in the liver without further modification, which is accordant with the imaging results *in vivo* MR. Besides, the nanoparticles are also found in spleen and kidney. The presence of Fe_3O_4@Gd nanoparticles in the kidney may suggest the nanoparticles could be cleared by kidney. Further pharmacokinetic studies of the nanoparticles at different time are necessary for a full understanding of the biodistribution.

Conclusions

A new kind of T_2-weighted MR imaging contrast agents based on Fe_3O_4 nanoparticles and Gd^{3+} ions were prepared. The introduction of Gd^{3+} increased the transverse relaxation rate of Fe_3O_4 nanoparticles but still maintained their good biocompatibility. Both *in vitro* and *in vivo* studies showed the nanoparticles had an obvious MR enhancement.

Conflicts of interest

The authors declare no conflict of interest.

Acknowledgements

This work was funded by the National Natural Science Foundation of China (Grant No. 51302004 to M.-M. S.), Anhui Provincial Natural Science Foundation of China (Grant No. 1308085QH141 to M.-M. S.) and University Natural Science Research Project of Anhui Province (Grant No. KJ2018A0172 to Y.-K. W.).

References

1 R. L. Siegel, K. D. Miller and A. Jemal, *Ca-Cancer J. Clin.*, 2020, **70**, 7–30.
2 O. Gobbo, K. Sjaastad, M. Radomski, Y. Volkov and A. Prina-Mello, *Theranostics*, 2015, **5**, 1249–1263.
3 M. Busquets, J. Estelrich and M.-J. Sánchez-Martín, *Int. J. Nanomed.*, 2015, **10**, 1727.
4 R. Weissleder and M. Pittet, *Nature*, 2008, **452**, 580–589.
5 E. Boros, E. M. Gale and P. Caravan, *Dalton Trans.*, 2015, **44**, 4804–4818.
6 Z. Li, P. Yi, Q. Sun, H. Lei, H. Zhao, Z. Zhu, S. Smith, M. Lan and M. Lu, *Adv. Funct. Mater.*, 2012, **22**, 2387–2393.
7 Z. Shen, A. Wu and X. Chen, *Mol. Pharm.*, 2017, **14**, 1352–1364.
8 W. Tang, Z. Zhen, C. Yang, L. Wang, T. Cowger, H. Chen, T. Todd, K. Hekmatyar, Q. Zhao, Y. Hou and J. Xie, *Small*, 2014, **10**, 1245–1249.
9 J.-H. Lee, Y.-M. Huh, Y.-w. Jun, J.-W. Seo, J.-T. Jang, H.-T. Song, S. Kim, E.-J. Cho, H.-G. Yoon, J.-s. Suh and J. Cheon, *Nat. Med.*, 2007, **13**, 95–99.
10 H. B. Na, I. C. Song and T. Hyeon, *Adv. Mater.*, 2009, **21**, 2133–2148.
11 Z. Zh, Z. Zhou, J. Bao, Z. Wang, J. Hu, X. Chi, K. Ni, R. Wang, X. Chen, Z. Chen and J. Gao, *Nat. Commun.*, 2013, **4**, 2266.
12 S.-H. Noh, W. Na, J.-T. Jang, J.-H. Lee, E. Lee, S. H. Moon, Y. Lim, J.-S. Shin and J. Cheon, *Nano Lett.*, 2012, **12**, 3716–3721.
13 K. Hayashi, M. Nakamura, W. Sakamoto, T. Yogo, H. Miki, S. Ozaki, M. Abe, T. Matsumoto and K. Ishimura, *Theranostics*, 2013, **3**, 366–376.
14 M. Wu, D. Zhang, Y. Zeng, L. Wu, X. Liu and J. Liu, *Nanotechnol*, 2015, **26**, 115102.
15 M.-Y. Fei, M.-M. Song, P. Wang, G.-z. Pang, J. Chen, D.-P. Lu, R. Liu, G.-Y. Zhang, T.-T. Zhao and Y.-Q. Yu, *RSC Adv.*, 2020, **10**, 5294–5303.
16 C. C. Huang, C. Y. Tsai, H. S. Sheu, K. Y. Chuang, C. H. Su, U. S. Jeng, F. Y. Cheng, C. H. Su, H. Y. Lei and C. S. Yeh, *ACS Nano*, 2011, **5**, 3905–3916.
17 H. Yang, Y. Zhuang, Y. Sun, A. Dai, X. Shi, D. Wu, F. Li, H. Hu and S. Yang, *Biomaterials*, 2011, **32**, 4584–4593.
18 K. Luo, J. Tian, G. Liu, J. Sun, C. Xia, H. Tang, L. Lin, T. Miao, X. Zhao, F. Gao, Q. Gong, B. Song, X. Shuai, H. Ai and Z. Gu, *J. Nanosci. Nanotechnol.*, 2010, **10**, 540–548.
19 K. H. Bae, Y. B. Kim, Y. J. Lee, J. Hwang, H. Park and T. G. Park, *Bioconjugate Chem.*, 2010, **21**, 505–512.
20 L. Wang, J. Bao, L. Wang, F. Zhang and Y. Li, *Chem.–Eur. J.*, 2006, **12**, 6341–6347.
21 F. Li, D. Zhi, Y. Luo, J. Zhang, X. Nan, Y. Zhang, W. Zhou, B. Qiu, L. Wen and G. Liang, *Nanoscale*, 2016, **8**, 12826–12833.
22 H. Cai, X. An, S. Wen, J. Li, G. Zhang, X. Shi and M. Shen, *Part. Part. Syst. Charact.*, 2015, **32**, 934–943.
23 N. Thorat, R. Bohara, H. Yadav and T. Syed, *RSC Adv.*, 2016, **6**, 94967–94975.
24 N. Thorat, R. Bohara, S. Tofail, Z. Alothman, M. Shiddiky, S. Hossain, Y. Yamauchi and K. Wu, *Eur. J. Inorg. Chem.*, 2016, **16**, 4586–4597.
25 A. Szpak, S. Fiejdasz, W. Prendota, T. Straczek, C. Kapusta, J. Szmyd, M. Nowakowska and S. Zapotoczny, *J. Nanopart. Res.*, 2014, **16**, 2678.
26 W. Zhang, L. Liu, H. Chen, K. Hu, I. Delahunty, S. Gao and J. Xie, *Theranostics*, 2018, **8**, 2521–2548.